Hydrogen diffusion, complex formation, and dissociation in acceptor-doped silicon carbide

M. S. Janson,[1] A. Hallén,[1] M. K. Linnarsson,[1] and B. G. Svensson[1,2]
[1]*Royal Institute of Technology, Institute of Microelectronics and Information Technology, P.O. Box E229, SE-164 40 Kista-Stockholm, Sweden*
[2]*University of Oslo, Physics Department/Physical Electronics, P.B. 1048 Blindern, N-0316 Oslo, Norway*
(Received 14 May 2001; published 15 October 2001)

The diffusion of deuterium (^{2}H) in B and Al doped 4*H* and 6*H* silicon carbide (SiC) has been studied in detail by secondary ion mass spectrometry. From ^{2}H depth profiles, following trap limited diffusion with negligible complex dissociation, an effective capture radius for the formation of ^{2}H-B complexes (at 460 °C) is determined to $R^{HB}=(21\pm4)$ Å. This value is in good agreement with that expected for a Coulomb force assisted trapping mechanism. At annealing conditions where dissociation is non-negligible, the ^{2}H diffusion follows Fick's law with a constant effective diffusivity, from which the complex dissociation frequencies ν are determined. The extracted values of ν cover three orders of magnitude and exhibit a close to perfect Arrhenius temperature dependence for both ^{2}H-B and ^{2}H-Al complexes. The large difference between the extracted complex dissociation energies, $E_d^{HB}=(2.51\pm0.04)$ eV and $E_d^{HAl}=(1.61\pm0.02)$ eV, suggests that the atomic configurations of the two complexes are significantly different. The corresponding extracted dissociation attempt frequencies, $\nu_0^{HB}=(1.2\pm0.7)\times10^{13}\,s^{-1}$ and $\nu_0^{HAl}=(0.7\pm0.3)\times10^{13}\,s^{-1}$, are very close to the characteristic oscillation frequency of the SiC lattice, $\nu_{lattice}^{SiC}=1.6\times10^{13}\,s^{-1}$. This is strong evidence for the assumption of a first order dissociation process. No difference between 4*H*- and 6*H*-SiC has been observed.

DOI: 10.1103/PhysRevB.64.195202 PACS number(s): 66.30.Jt, 66.30.Xj, 82.80.Ms

I. INTRODUCTION

Hydrogen (H) has been extensively studied in semiconductors since the 1950s, but the ability of hydrogen to electrically passivate shallow acceptors and donors was not discovered until the early 1980s. Theoretical studies, supported by several experimental observations, have further shown that isolated hydrogen also behaves as a negative U center in many semiconductors. This means that an uncontrolled presence of hydrogen in a semiconductor material may be detrimental for device performance. On the other hand, H may also be used beneficially for example for passivation of interface-trapped charge of a MOS transistor. Due to this strong influence—positive or negative—knowledge of the hydrogen diffusion properties is of crucial importance to any semiconductor technology. For further reviews on these topics see, e.g., Refs. 1 and 2.

In a typical diffusion experiment, H is introduced to the semiconductor from a hydrogen plasma or using low energy H^+ ion implantation. The sample is then subjected to various thermal treatments and finally the distribution of H is measured either directly [e.g. using secondary ion mass spectrometry (SIMS)], or by registering the combined effects of H passivation and compensation through electrical techniques such as capacitance-voltage (CV) measurements.

The solubility for isolated interstitial H at temperatures below ~1000 °C has been found to be very low in most semiconductors, and the overwhelming majority of the H atoms appears in the form of—more or less—immobile H defect, or H-H complexes.[1] As a consequence, the measurable effective mobility of H is not primarily determined by the diffusivity of the mobile H atoms, but rather by the formation and dissociation properties of the dominating H-defect complex.

Two classes of experiments have been used to determine the dissociation energy of a H-defect complex. In the first, prehydrogenated samples are thermally annealed in the presence of a strong electric field supplied by a reversed biased *p-n* or Schottky diode at the sample surface. The charged H atoms, released from H-defect complexes, are then swept out of the surface region by the applied field, minimizing the recapture of H. In this way the H-defect complex dissociation frequency ν is directly obtained from the reduction rate of H close to the surface, providing it follows first order kinetics. The drawback of this method is that the electric field may influence the trapping/dissociation kinetics and that it also must be shown that the recapture of H can be neglected. The second class of experiment exploits the fact that the diffusion of H in a trap rich material (without an electric field) is entirely limited by the trapping and dissociation processes. The dissociation frequency can then be calculated from the measured effective H diffusion constant provided that the trap concentration and the effective capture radius *R* of the complex are known. In practice, this is only possible if *R* has a small temperature dependence. Fortunately, for trapping of mobile H^+ at ionized acceptors *R* is determined by long range coulomb attraction and can therefore be expected to have a small temperature dependence. Zundel and Weber have employed the two different experimental procedures in two independent studies of the H-B complex in Si (Refs. 3 and 4) and obtained identical dissociation energies for the complex.

Silicon carbide (SiC) is a close packed material with equal amount of Si and C atoms whose strong covalent/ionic Si-C bonds give rise to its superior properties for different technological applications. SiC is a very hard material and has—under the name carborundum—been used as an abrasive substance for over 100 yr.[5] SiC is thermally stable up to 2700 °C and is, therefore, used as a protective coating in various high temperature applications. Being a low-*Z* refrac-

tory material with good thermal shock resistance SiC is an aspirant as a first wall material in fusion plasma devices.[6] SiC is also a semiconductor, characterized by a wide bandgap, large breakdown electric field, high saturation electron velocity and an extremely high thermal conductivity. These properties make SiC a prime candidate for a new generation of high power, high frequency, and high temperature devices. The high chemical stability and radiation tolerance also make SiC suitable for sensor applications in harsh environments.[7]

Hydrogen is expected to be a major impurity in epitaxial SiC layers due to its presence in the epitaxial precursor gases $[SiH_4, C_3H_8, Al(CH_3)_3]$ and since H_2 is used as carrier gas during growth.[8] Indeed, high concentrations of H have been observed—by SIMS and low temperature photoluminescence (LTPL)—in *p*-type,[9,10] and—by nuclear reaction analysis and infrared absorption measurements—in *n*-type[11] epitaxial layers. These studies also showed that a postgrowth anneal in Ar atmosphere at temperatures $\geqslant 1000\,^{\circ}C$ reduced the H content in the (*p*-type) layers, while the carrier concentration increased. This was a first indication of H induced acceptor passivation in SiC. In 1995, Gendron and Clerjaud *et al.*[12,13] demonstrated a decrease in the carrier concentration with a corresponding drop of the N, B, and Al related electron spin resonance (ESR) spectra in samples subjected to a H_2 anneal at 1600 °C and 10 bar. This was attributed to formation of H-dopant complexes since the ESR spectra of the virgin samples were recovered for the hydrogenated samples by a second anneal in a He atmosphere. On the other hand, in a subsequent experiment under the same experimental conditions as in Ref. 12, but with lighter N-doped material no donor passivation was found.[14]

Acceptor and donor passivation in SiC has also been studied using H plasma treatments.[15–18] In general these investigations show that passivation can be obtained in *p*-type material while the effect on *n*-type SiC is small. This passivation effect can not, however, be entirely assigned to the formation of H-acceptor complexes since substitution of the H plasma to that of He or Ar has given similar results.[15,18]

Further evidence for B and Al passivation by H has, however, been given in the works of Linnarsson *et al.*,[19–21] Achtziger *et al.*,[22,23] Hülsen *et al.*,[24] and Janson *et al.*[25] In the majority of these experiments H was introduced into the material using low energy ^1H or ^2H ion implantation while the H distributions were recorded by SIMS and/or CV measurements. The major results of these works can be summarized as follows: H passivates both Al and B where the H-B complex is more thermally stable than H-Al.[19,20,22] The reactivation of passivated acceptors under a reverse biased Schottky diode,[23] and the H diffusion kinetics in the presence of a large doping gradient,[26] show that mobile H has a positive charge state in *p*-type SiC. The reactivation kinetics give an upper limit of 1.8 eV for the H-Al dissociation energy[24] which is in accordance with our recently published value of (1.66 ± 0.05) eV, obtained from effective diffusivity experiments.[25] The reactivation process is faster for ^1H than for ^2H passivated Al-doped samples,[24] possibly indicating an isotope shift in the dissociation frequency. It has also been demonstrated[21] that H can be incorporated into *p*-type SiC, coated with a thin Ni or Pt film, directly from a H_2 containing ambient at temperatures $\geqslant 600\,^{\circ}C$. No hydrogen was found in samples with a Au or Ti coating or in samples with a bare SiC surface. Furthermore, no H was observed in *n*-type samples irrespective of metal coating and annealing temperature (up to 800 °C). This is also true for experiments using implanted H,[22] i.e., no donor passivation has been observed in any of these experiments.

Other studies of H diffusion in SiC include the early works of Causey *et al.*[27] They determined the H diffusion constant by measuring the release rate of gaseous tritium (^3H) during thermal annealing of different SiC materials hydrogenated by recoil injected ^3H. For highly Al-doped monocrystalline SiC they obtained an activation energy of (1.5 ± 0.2) eV for diffusion, while the corresponding values for (relatively) low doped material were typically 1 eV higher.

Ab initio calculations regarding H in SiC have so far been devoted to interstitial H[28,29] and to H-vacancy complexes.[29,30] Deak, Gali, and Aradi[29] predicted a negative U behavior of interstitial hydrogen in 4*H*-SiC with the $(+/-)$ level situated 2.25 eV above the valence band edge, in accordance with the experimental observations of a H^+ state in *p*-type SiC. The most stable form of noncomplexed H in *n*-type material was predicted to be H_2.[29] This could explain the difficulty to observe H diffusion and passivation in *n*-type SiC.

In this work we focus on the diffusion of H in acceptor doped SiC. The aim is to establish the diffusion kinetics and to accurately determine the dissociation energies of the passivating H-B and H-Al complexes. H was introduced using ion implantation while the H profiles were determined by SIMS. Deuterium (^2H) was used throughout the study since the sensitivity for ^2H is $\sim 10^3$ times higher than for ^1H in the SIMS measurements. To extract the parameters from the experimental data we make extensive use of the theory for trap limited diffusion. To make this present article more comprehensive we have included a detailed description of this theory adapted to our experimental conditions. This is done in the next section (Sec. II). Section III outlines the experimental procedure while we present and discuss the experimental results in Sec. IV.

II. KINETICS OF TRAP LIMITED DIFFUSION

Diffusion of mobile atoms *A* including the formation of immobile complexes *AB* at immobile trapping centers *B* and the subsequent dissociation of these complexes,

$$A + B \leftrightarrow AB \tag{1}$$

can be formulated mathematically using Fick's second law of diffusion[31] and first order reaction kinetics. When the total concentration of traps $B_{tot}=[B]+[AB]$ remains constant over time, the trap-limited diffusion is described by two coupled differential equations (brackets denote concentration values),

$$\frac{\partial[A]}{\partial t}=\frac{\partial}{\partial x}\left(D_A\frac{\partial[A]}{\partial x}\right)-\frac{\partial[AB]}{\partial t}, \tag{2a}$$

$$\frac{\partial[AB]}{\partial t}=K[A][B]-\nu[AB],$$

$$[B]=B_{\text{tot}}-[AB],$$

$$K=4\pi RD_A, \tag{2b}$$

where t is the time and D_A is the (intrinsic) diffusion coefficient for A. The expression for the complex formation rate constant K is given by the theory of bimolecular reaction rates in solids[32] in which R is the effective capture radius of the trap B and is usually set to a value of the same order as the interatomic distance in the lattice. However, in the case of trapping of charged atoms at traps of opposite charge (as in the trapping of H^+ at an ionized acceptor) one would anticipate a considerably larger R due to Coulomb attraction. This reaction radius R_c is often estimated as the distance between the (singly) charged A^+ and B^- where the Coulomb potential energy loss equals the thermal energy,

$$\frac{e^2}{4\pi\varepsilon R_c}=k_BT \quad (\text{SI units}), \tag{3}$$

where e is the elementary charge, ε the dielectric constant, k_B Boltzmann constant, and T absolute temperature. Equation (3) originates from the theory of recombination in gases[33] and the direct adaptation to solid state diffusion has not been thoroughly investigated. ν in Eq. (2b) is the complex dissociation frequency of the complex and is expected to follow an Arrhenius temperature dependence

$$\nu=\nu_0\exp\left(-\frac{E_d}{k_BT}\right), \tag{4}$$

where ν_0 is the so called attempt frequency and E_d is the dissociation energy of the complex. ν_0 should in turn be of the same order of magnitude as the characteristic oscillation frequency of the lattice, ν_{lattice}, which may be calculated by weighing each vibration mode ω_k with the energy of that mode,

$$\nu_{\text{lattice}}=\frac{1}{2\pi}\langle\omega\rangle=\frac{1}{2\pi}\frac{\Sigma_k\omega_k(\omega_k\hbar\langle n\rangle)}{\Sigma_k(\omega_k\hbar\langle n\rangle)}. \tag{5}$$

Here $\langle n\rangle$ is the Planck distribution function, and $\hbar$ the reduced Planck constant. Typical values for ν_{lattice} are in the low $10^{13}\,\text{s}^{-1}$ range and depend on the Debye temperature θ_D. Numerical integration of Eq. (5), with the dispersion relation given by the Debye approximation ($\theta_D^{\text{SiC}}=1120\,\text{K}$),[34] yields an oscillation frequency for SiC of $\nu_{\text{lattice}}^{\text{SiC}}=1.6\times10^{13}\,\text{s}^{-1}$ at 600 K, and is nearly independent on temperature above ~300 K.

The solution to Eq. (2), with a given set of boundary and initial conditions, can generally only be accomplished numerically. Even the standard problems, i.e., an infinite source at the surface or an initial Gauss distribution, lack general analytical solutions. Analytical solutions may, nevertheless, be found for limited regimes of Eq. (2) following appropriate simplifications (see Refs. 2, 4 and 35).

A major simplification is the assumption of local equilibrium (LE) in reaction (1), which means that the process of balancing the complex formation and dissociation rates is much faster than the spatial change of any of the constituents. With $\partial[AB]/\partial t\approx0$ in Eq. (2b), the balance equation becomes

$$[AB]^{\text{LE}}=\frac{B_{\text{tot}}}{1+\nu/(K[A]^{\text{LE}})}, \tag{6}$$

where the LE superscripts refer to local equilibrium values. It is difficult to find a general condition for the validity of LE, but a rule-of-thumb states that the time needed for a nonequilibrium system to reach LE (as in the initial stage of a heat treatment) is on the order of $1/\nu$. Numerical simulations show that this is usually a rather conservative constraint.

Equation (2) may be divided into two regimes depending on the magnitude of ν: (A) a regime with a high dissociation constant, and (B) a regime with negligible dissociation. These cases are considered below.

A. High dissociation regime

From Eq. (6) is it seen that for sufficiently high complex dissociation frequencies, ν, the LE concentration of complexes will be much smaller than the concentration of traps and vice versa:

$$\nu/(K[A]^{\text{LE}})\gg1\Leftrightarrow[AB]^{\text{LE}}\ll B_{\text{tot}}. \tag{7}$$

Under the constraint set by Eq. (7), Eq. (6) can be simplified to

$$[AB]^{\text{LE}}=\frac{KB_{\text{tot}}}{\nu}[A]^{\text{LE}}. \tag{8}$$

Equation (2) can now be greatly simplified. Substitution of Eq. (8) in Eq. (2a) and introducing $[A_{\text{tot}}]=[A]+[AB]$ gives

$$\frac{\partial[A_{\text{tot}}]}{\partial t}=D_{\text{eff}}\frac{\partial^2[A_{\text{tot}}]}{\partial x^2},$$

$$D_{\text{eff}}=\frac{D_A}{1+KB_{\text{tot}}/\nu}=D_A\frac{[A]}{[A_{\text{tot}}]}, \tag{9}$$

where we have assumed a constant D_A and a homogenous trap concentration B_{tot}. The total concentration of A's is thus expected to diffuse according to Fick's law with a constant effective diffusion coefficient D_{eff}. (The use of $[A_{\text{tot}}]$ here is motivated by the fact that the SIMS technique provides total chemical concentrations.)

It is evident from Eq. (9) that D_{eff} in turn can be divided in two regimes depending on the ratio $\nu/(KB_{\text{tot}})$. At very high dissociation frequencies the mobile A's will dominate over the complex concentration and

$$D_{\text{eff}}=D_A,$$

$$(\nu/(KB_{\text{tot}})\gg1\Leftrightarrow[A]^{\text{LE}}\gg[AB]^{\text{LE}}). \tag{10a}$$

At more moderate ν, but still high enough to satisfy Eq. (7), the complexes are the dominating species and D_{eff} becomes entirely determined by the trapping/dissociation process, independent on D_A:

$$D_{\text{eff}} = \frac{\nu}{4\pi R B_{\text{tot}}},$$

$$(\nu/(KB_{\text{tot}}) \ll 1 \Leftrightarrow [A]^{\text{LE}} \ll [AB]^{\text{LE}}). \tag{10b}$$

A simple picture to illustrate this independence is that the average time between detrapping and retrapping of an A is negligible compared to the average lifetime of a complex.

An experimental consequence of Eqs. (8) and (10b) is that D_A cannot be extracted at temperatures where the major part of the mobile species is present in the form of complexes ($[AB] \approx [A_{\text{tot}}]$), unless the concentration of untrapped A's is established. Unfortunately, this is usually not possible. This is the reason for the great difficulty to extract the intrinsic diffusion constant for hydrogen in Si at temperatures $\leqslant 1000\,^{\circ}\text{C}$.[35] On the other hand, by the use of Eq. (10b), it is possible to determine the dissociation energy of a complex from measurements of the H diffusion.

B. Negligible dissociation regime

At low temperatures, dissociation is negligible and the LE complex concentration becomes essentially equal to the trap concentration, $[AB]^{\text{LE}} \approx B_{\text{tot}}$, assuming a non-limiting source of A's. As seen in Eq. (6) this occurs when

$$\nu/(K[A]^{\text{LE}}) \ll 1. \tag{11}$$

Without dissociation, diffusion of A's will only take place with a renewed supply of A's or with an initial concentration of A's exceeding the initial trap concentration. The problem studied here will be with an infinite source of A's at the surface

$$[A]_{x=0} = A_0, \tag{12}$$

a homogeneous trap concentration B_{tot} ($A_0 \ll B_{\text{tot}}$), and with the initial condition $[A_{\text{tot}}]_{t=0} = 0$. Initially, complexes start to build up close to the surface and at this early stage, when the complex concentration has not yet reached the trap concentration, $[AB] \ll B_{\text{tot}}$, Eq. (2b) can be simplified to

$$\frac{\partial [AB]}{\partial t} = KB_{\text{tot}}[A]. \tag{13}$$

Substitution of Eq. (13) in Eq. (2a) gives a steady state solution, $\partial [A]/\partial t \approx 0$, which, together with the boundary condition (12) becomes

$$[A] = A_0 \exp(-\alpha x),$$

$$\alpha = \sqrt{B_{\text{tot}} 4\pi R}. \tag{14}$$

Furthermore, substitution of Eq. (14) in Eq. (13) and integration gives the expression for the total concentration of A's

$$[A_{\text{tot}}] = (1 + KB_{\text{tot}} t) A_0 \exp(-\alpha x). \tag{15}$$

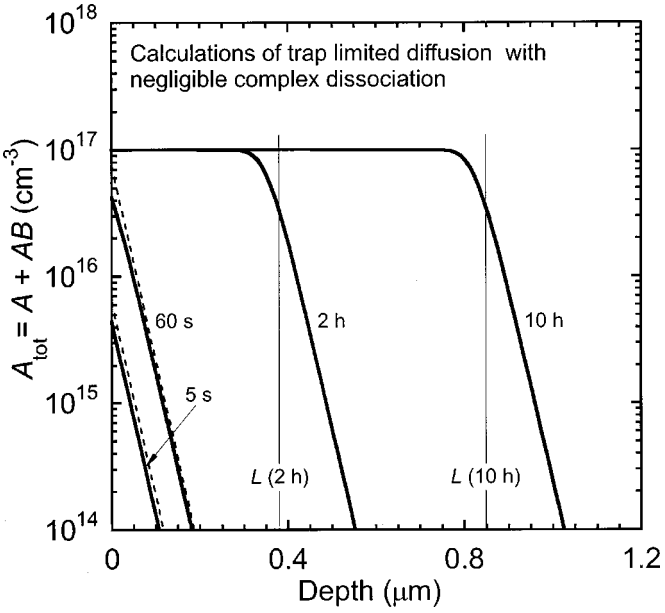

FIG. 1. An example of numerical solutions (thick solid lines) to Eq. (2) ($D_A = 10^{-10}\,\text{cm}^2/\text{s}$, $R = 10\,\text{Å}$, $\nu = 10^{-5}\,\text{s}^{-1}$) with boundary condition Eq. (12) ($A_0 = 10^{14}\,\text{cm}^{-3}$) and homogenous trap level $B_{\text{tot}} = 10^{17}\,\text{cm}^{-3}$. Diffusion times t are 5 s, 60 s, 2 h, and 10 h. Dissociation of formed complexes is negligible according to condition Eq. (11) since $\nu/(KA_0) = 8 \times 10^{-4} \ll 1$. The analytical solutions [Eq. (15)] for $t = 5$ and 60 s (dashed lines) are in good agreement with the numerical results as is the analytical prediction [Eq. (18)] for the thickness of the saturated layer L (thin vertical lines).

Figure 1 shows numerically calculated $[A_{\text{tot}}]$ profiles, and their analytical counterparts for a system with negligible dissociation [$\nu/(KA_0) = 8 \times 10^{-4} \ll 1$] and with an infinite source of A's at $x = 0$. The numerical and analytical [Eq. (15)] results are in good agreement for $t = 5$ and 60 s, which is to be expected since $[AB] \approx [A_{\text{tot}}] \ll B_{\text{tot}}$. When the complex concentration approaches the trap concentration $B_{\text{tot}} = 10^{17}\,\text{cm}^{-3}$, $[A_{\text{tot}}]$ flattens out and further diffusion results in the development of a saturated layer of thickness L ended by an exponential diffusion front. Although no formal analytical solution has been obtained in this regime, $L(t)$ can be calculated by considering that the region of the diffusion front acts as a sink for the A's and that the A's diffuse unaffected by the saturated traps from the source to this sink. Assuming a perfect sink, the flux of A's through the saturated layer becomes

$$F = -D_A \frac{(0 - A_0)}{L}. \tag{16}$$

This flux must, however, be balanced by the flux needed to gradually saturate the free traps B at the diffusion front

$$F = B_{\text{tot}} \frac{\partial L}{\partial t}. \tag{17}$$

The differential equation constituted by Eqs. (16) and (17) yields the solution

TABLE I. Sample name, SiC polytype, B and Al concentrations (determined by SIMS) of the epitaxial layers used in this study.

Sample	Polytype	[B] (cm^{-3})	[Al] (cm^{-3})
B1	4*H*	9.6×10^{16}	3.4×10^{16}
B2	4*H*	1.4×10^{17}	1.4×10^{17}
B3	4*H*	5.0×10^{17}	1.7×10^{17}
B4	6*H*	8.1×10^{16}	1.8×10^{16}
Al1	4*H*	2×10^{15}	2.4×10^{18} Buried layer

$$L=\sqrt{\frac{2D_AA_0}{B_{\mathrm{tot}}}t}. \tag{18}$$

This result is represented in Fig. 1 as vertical lines and agrees with the numerical calculations. An important observation from Fig. 1 is that the steep fronts following the saturated layers have the same exponential slopes α as in the profiles of the initial diffusion phase, given by Eq. (14). This can, at least intuitively, be understood by the fact that a homogenous flux of *A*'s through the layer, given by Eq. (16), in combination with an absence of free traps *B*, will cancel all the right-hand terms in Eqs. (2a) and (2b) between the surface and front region. The essential difference between the initial stage described by Eq. (14) and the subsequent diffusion front, is then the concentration of *A*'s. However, α in Eq. (14) is independent on $[A]$ (or A_0) and the slopes of the two profiles will be the same.

Unfortunately, Eqs. (15) and (18) reveal the same problem regarding the determination of D_A as noted above for the case of moderate ν, i.e., D_A can not be determined without specific knowledge about $[A]$ (or A_0).

III. EXPERIMENT

A. Sample preparation

For the study of ^{2}H-B interaction, three 4*H*- (B1–B3), and one 6*H*- (B4), SiC epitaxial layers were used. These layers were doped with B in the low to mid $10^{17}\,cm^{-3}$ range and also contained Al to equal or somewhat smaller amounts. For the ^{2}H-Al study, a 4*H*-SiC epitaxial structure (Al1) with a buried Al layer doped to the mid $10^{18}\,cm^{-3}$ range was used. The buried Al layer had a thickness of 1 μm, starting at 1 μm below the sample surface. Al1 also contained a small amount of B, homogeneously distributed with a concentration of $2\times10^{15}\,cm^{-3}$. The epitaxial layers were grown in a horizontal CVD reactor, described in detail elsewhere.[8] Table I lists the B and Al concentrations (as determined by SIMS) as well as the polytype of each epitaxial layer.

Deuterium was introduced into the layers by implanting 10 keV $^2H^+$ ions at 300 K to a dose of $1\times10^{15}\,cm^{-2}$. The energy was chosen such that the implantation profile would not extend into the buried Al layer of Al1. The epilayers were then heat treated in a first annealing step in order to diffuse some of the implanted ^{2}H deeper into the layers. Two sets of the B1–B4 samples were annealed at 460 °C for 30 min and 2 h, respectively, while the Al1 sample was heat treated at 300 °C for 30 min. The annealings were performed in a resistively heated vacuum furnace with a base pressure in the low 10^{-7} Torr range and with a temperature accuracy of $\Delta T\leqslant5$ °C. Subsequently, the implanted surface layer was etched off using an inductively coupled plasma (ICP) etch system with a SF_6 plasma. The epilayers were finally cut into smaller pieces which were further annealed at 470–620 °C (B1, B2, and B4), and at 270–400 °C (Al1). The durations of the anneals varied between 30 min and 146 h, and two anneal times differing by a factor of four, were performed at each temperature.

B. Measurement technique

The atomic concentration versus depth profiles were obtained by SIMS utilizing a Cameca IMS 4*f* microanalyzer. A primary sputtering beam of 8 keV $(^{16}O)_2^+$ ions (for Al and B) or 13.5 keV $^{133}Cs^+$ ions (^{2}H), was rastered over an area of $200\times200\,\mu m^2$. The erosion rate was typically 10 and 25 Å/s in the Cs and O_2 measurements, respectively. Secondary ions of $^{27}Al^+$, $^{11}B^+$, or $^2H^-$ were collected from an area, 60 μm in diameter, in the center of the sputtered crater. The total boron concentration in the epitaxial layers was assumed to be 25% higher than that of ^{11}B in order to account for the ^{10}B isotope. The use of ^{2}H instead of ^{1}H is due to the fact that the sensitivity for the former isotope is three orders of magnitude higher than for the latter. The SIMS background concentrations were typically $10^{15}\,cm^{-3}$, $10^{14}\,cm^{-3}$, and $10^{14}\,cm^{-3}$ for ^{2}H, ^{11}B, and ^{27}Al, respectively.

A frequent problem in SIMS analysis of implanted nonannealed, or highly passivated SiC, is sample charging. To minimize this effect a thin gold layer (~20 nm) was deposited on the samples in order to increase the surface conductivity. Moreover, electron flooding was employed during the O_2 measurements to further compensate the charging by the primary beam. The depth of the sputtered craters were measured using an Alphastep-200 stylus profilometer giving an uncertainty ⩽3% in the depth of the converted profiles. Calibration to absolute concentration values was carried out by measuring implanted standard samples along with the other samples. Under stable conditions, the accuracy in concentration was limited by the accuracy in the given implanted dose of the standard samples, ~20%. To ensure stable measurement conditions a matrix signal, related to Si and/or C, always accompanied the other signals. For the measurements where absolute concentration values were vital, variations in the matrix signal between the measured and standard samples did not exceed 10%. We should also mention that no samples subjected to SIMS measurements were further used in the investigation. This was done as a precaution since a recent study[36] have shown that a ^{1}H related photo luminescence spectra appeared in some SiC samples subjected to SIMS analysis. This SIMS induced ^{1}H is localized to the surface region only (⩽0.1 μm) but further annealing could release this ^{1}H and thereby disturb the ^{2}H diffusion characteristics.

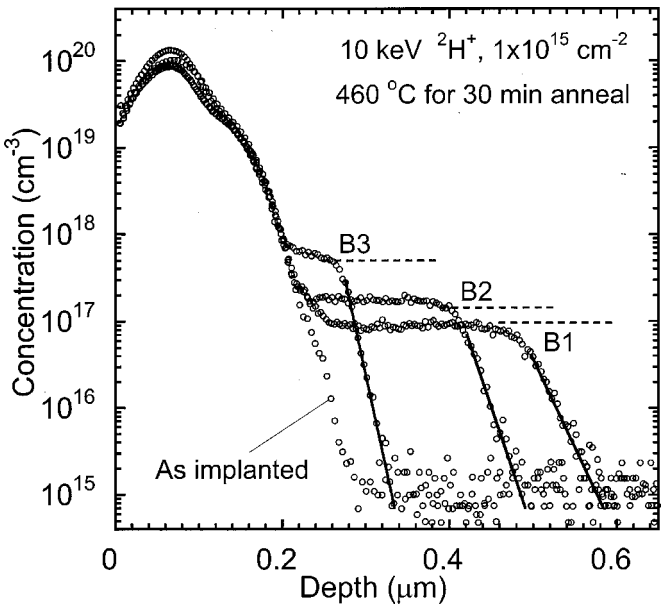

FIG. 2. SIMS measurements of ^{2}H concentration versus depth (○) in the ^{2}H implanted B1, B2, and B3 samples, as implanted and annealed at 460 °C for 30 min. The B concentration in each sample is indicated by the horizontal dashed lines. The solid lines represent least square fits of exponential functions to the diffusion fronts.

IV. RESULTS AND DISCUSSION

A. Hydrogen-acceptor complex formation

Figure 2 shows concentration versus depth profiles of ^{2}H in the B1, B2, and B3 samples, as implanted and annealed at 460 °C for 30 min. The as implanted profile has a maximum concentration at 0.06 μm and exhibits a shoulder starting at 0.12 μm. This type of profile is not expected for a single energy ''random''direction implant and the reason for this anomalous shape is still unclear although channeling could play some role. However, the detailed shape of the implantation profile is of little importance to this study since the implanted ^{2}H is only used as a diffusion source. During the annealing at 460 °C ^{2}H diffuses deeper into the samples and profiles with a constant concentration, closely correlated to the B concentration in each sample, appear. The constant concentration profiles are followed by steep exponential diffusion fronts with steeper slopes for samples with higher B doping while the in-diffused depth of the profiles are inversely dependent on the B content. Figure 3 displays the temporal development of the implanted and 460 °C annealed B1 samples. The ^{2}H diffusion profile of the sample annealed for 2 h reaches 20% deeper than that annealed for 30 min. Furthermore, both profiles exhibit exponential diffusion fronts with parallel exponential slopes. With the recent proofs for the existence of a passivating H-B complex in SiC,[12,19,22] the profiles in Figs. 2 and 3 are interpreted as diffusion of ^{2}H out of the implanted region with subsequent formation of nondissociating ^{2}H-B complexes. The close correlation between the ^{2}H and B concentrations also suggest that the concentration of the migrating ^{2}H, as well as of any existing ^{2}H-Al complexes, is lower than the ^{2}H-B complex concentration. With a seemingly large source of ^{2}H in the surface region, the diffusion profiles of Figs. 2 and 3 should follow the kinetics of trap limited diffusion with negligible dissociation and with an infinite diffusion source, as described in Sec. II B. However, even though the penetration depths L^H of the ^{2}H profiles in Fig. 2 do qualitatively have the [B] dependence as predicted by Eq. (18), the weak t dependence of L^H (Fig. 3) shows that the source of ^{2}H is far from ideal (i.e., constant concentration over time). This is due to the fact that only a very small fraction of the implanted ^{2}H is free to migrate into the samples at the present temperatures. A redistribution of implanted ^{1}H has been found to take place with an activation energy of 3.5 eV,[37] while the activation energy of the (first order) out diffusion of implanted ^{2}H has been determined to 4.9 eV.[38] These relatively high activation energies for the H mobility in the im-

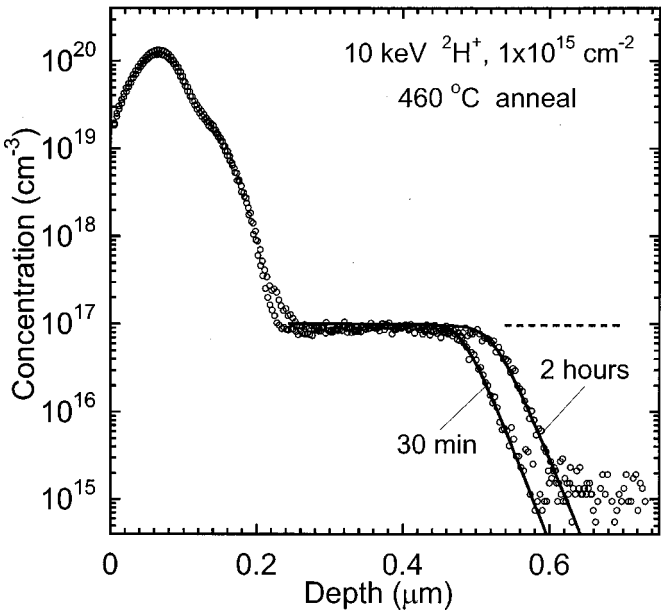

FIG. 3. SIMS measurements of ^{2}H concentration versus depth (○) in the ^{2}H implanted B1 sample, annealed at 460 °C for 30 min and 2 h, respectively. The B concentration is indicated by the horizontal dashed line. The solid lines represent numerical simulations of the trap limited ^{2}H diffusion as described in Sec. IV B.

TABLE II. Exponential slopes α of the ^{2}H diffusion fronts extracted from the ^{2}H implanted B1–B4 samples annealed in vacuum at 460 °C for 30 min or 2 h. The effective capture radius of the ^{2}H-B complex R^{HB} are calculated, using Eq. (14), from α and the B concentrations listed in Table I.

Sample	Anneal time	α (10^5 cm^{-1})	R^{HB} (Å)
B1	30 min	4.7	18
	2 h	5.2	22
B2	30 min	6.6	24
	2 h	6.4	23
B3	30 min	10	16
	2 h	12	23
B4	30 min	4.6	21

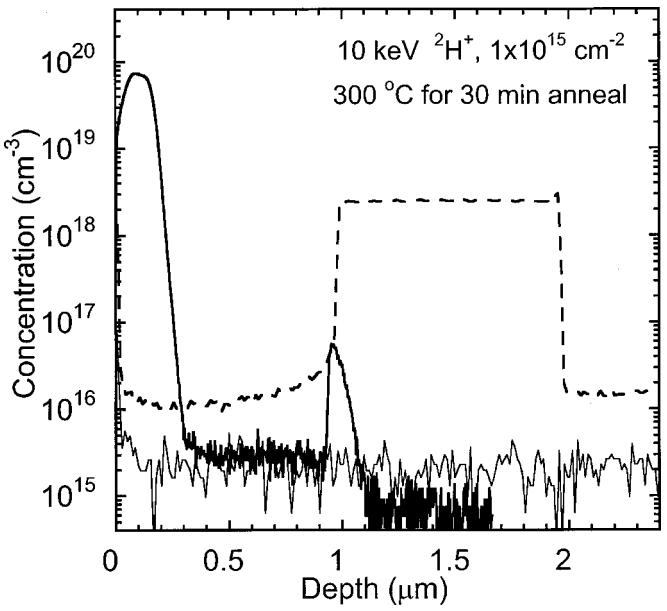

FIG. 4. Concentrations versus depth from SIMS measurements of ^{2}H (solid line), ^{27}Al (dashed line), and B (thin solid line) in the ^{2}H implanted Al1 sample, annealed at 300 °C for 30 min. The B signal represent 1.25×[^{11}B] to account for the natural abundance of ^{10}B.

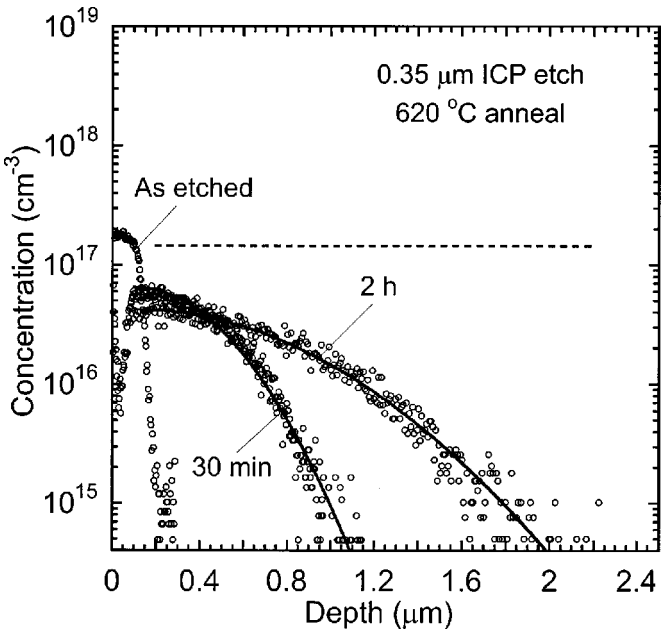

FIG. 5. SIMS measurements of ^{2}H concentration versus depth (○) in the ^{2}H implanted, initially annealed (460 °C for 2 h), and 0.35 μm ICP etched B2 sample, as etched and annealed at 620 °C for 30 min and 2 h, respectively. The B concentration is indicated by the horizontal dashed line. The solid lines represent least square fits of Gaussian functions to the diffusion profiles. The ^{2}H background concentration of $1\times10^{15}\,\mathrm{cm}^{-3}$ has been subtracted from the ^{2}H profiles in the figure prior to the Gaussian fitting procedure.

planted region, presumably due to the trapping and detrapping of H at implantation induced defects, results in a decreasing ''surface'' concentration of ^{2}H during the present heat treatments.

In contrast to L, the expression for the slope α of the exponential diffusion front, Eq. (14), does not depend on the concentration of the diffusing species and may, therefore, exhibit a better agreement with the experimental results. It should be noted, however, that even though α does not explicitly depend on the ^{2}H concentration it may, in principle, be sensitive to a nonconstant diffusion source, as investigated in Sec. IV B by numerical simulations. The exponential slopes are extracted from the central parts of the diffusion fronts in each sample and are listed in Table II. The ^{2}H background concentration ($\sim1\times10^{15}\,\mathrm{cm}^{-3}$) was subtracted from the SIMS profiles prior to this extraction. The least square exponential fits are plotted in Fig. 2 as solid lines and show both the exponential nature of the profiles as well as qualitatively confirming Eq. (14), i.e., steeper fronts for higher trap concentrations. Table II shows that the slopes remain constant—within the experimental accuracy—when increasing the annealing time from 30 min to 2 h, confirming the negligible dissociation of the ^{2}H-B complexes. The effective capture radius for formation of the ^{2}H-B complex (at 460 °C) R^{HB} is then calculated from the extracted α, using Eq. (14) with B_{tot}=[B] in each sample. The extracted values of R^{HB} are listed in Table II and scatter somewhat although this scatter appears to be uncorrelated to the annealing time and the B concentration. Averaging over all values gives $R^{\mathrm{HB}}=(21\pm4)$ Å. This value is in fact in close agreement with the theoretical value obtained from Eq. (3) at 460 °C: $R_c=23$ Å ($\varepsilon_r^{\mathrm{SiC}}=10$).

The relatively large spread in the measurements of R in combination with the narrow experimental temperature interval, imposed by the condition for negligible complex dissociation, makes it difficult to experimentally confirm the relatively weak temperature dependence of R_c. This is probably one reason why there are so few quoted values of R_c in the literature, and to the best of our knowledge only two contributions exists in the literature where the effective capture radius of a H-acceptor complex in a semiconductor has been determined independently; Zundel and Weber;[3] and Seager, Anderson and Brice, [35] obtained R^{HB} values in Si of (40 ± 4) Å and (45 ± 5) Å, at 80 °C and 25 °C, respectively. These values are also in good agreement with those predicted by Eq. (3); $R_c=40$ Å and 47 Å respectively ($\varepsilon_r^{\mathrm{Si}}=11.9$). Equation (3) appears therefore to give a comprehensive description of R, but more experimental data and a theoretical treatment including the specific nature of the solid state diffusion are needed for a more detailed understanding of a Coulomb force assisted reaction radius in crystalline matter.

The ^{2}H diffusion profile in the Al1 sample differs somewhat from those in Figs. 2 and 3 due to the use of a buried Al layer. Figure 4 shows the Al, B, and ^{2}H SIMS profiles of the Al1 epitaxial layer, implanted with 10 keV $^2H^+$ ions to a dose of $1\times10^{15}\,\mathrm{cm}^{-2}$ and annealed at 300 °C for 30 min. Here, the original implanted ^{2}H distribution is confined to the low doped surface layer of the sample and exhibits a similar anomalous profile as observed in the B1–B4 samples. During the anneal, a small amount of ^{2}H has migrated into the buried Al layer forming a well defined peak at the edge

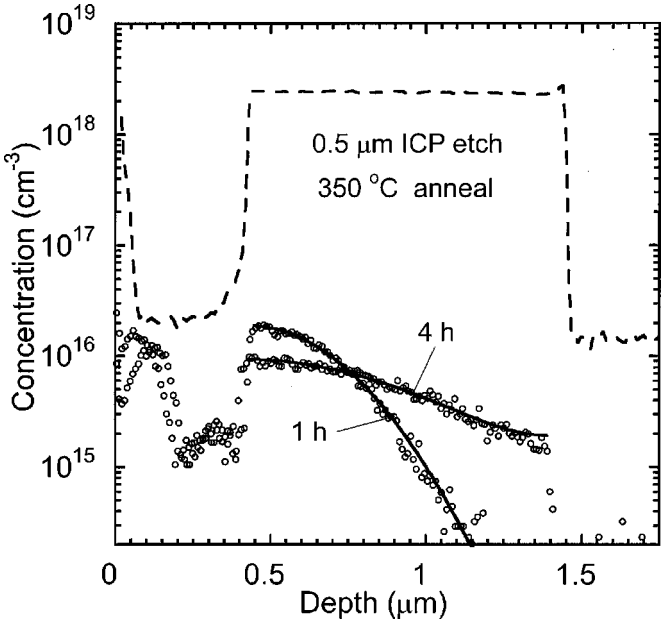

FIG. 6. Concentrations versus depth from SIMS measurements of ^{2}H (○), and ^{27}Al (dashed line) in the ^{2}H implanted, initially annealed (300 °C for 30 min), and 0.5 μm ICP etched Al1 sample, annealed at 350 °C for 1 h and 4 h, respectively. The solid lines represent least square fits of Gaussian functions to the diffusion profiles. (The sum of two Gaussians are used to account for the reflective boundary condition at $x=1.4\,\mu$m.) The ^{2}H background concentration of $1\times10^{15}\,\mathrm{cm}^{-3}$ has been subtracted from the ^{2}H profiles in the figure prior to the Gaussian fitting procedure.

of the layer. This accumulated ^{2}H peak suggests the formation of ^{2}H-Al complexes[12,22,25] but could also be caused by a segregation of positively charged ^{2}H in the presence of the built in electric field at the junction between the low and high doped acceptor layers.[26] However, in Sec. IV B we show that the majority of the ^{2}H in the buried layer consists of ^{2}H-Al complexes. A closer look at the profile of the ^{2}H peak shows that the front does not have an exponential decay. This implies that the complexes experience non-negligible dissociation at 300 °C, making an independent extraction of R^{HAI} impossible. The concentration of ^{2}H between the implanted region and the buried layer coincides with the homogenous B concentration in Al1 suggesting the presence of stable ^{2}H-B complexes.

B. Dissociation of H-acceptor complexes

To determine the ^{2}H-B and ^{2}H-Al dissociation energies we have used the implanted and ''primary'' annealed Al1, and B1, B2, and B4 samples (2 h anneal) described in Sec. IV A. To obtain well defined initial conditions for the further diffusion steps, the surface layers of the samples were etched off, including all ^{2}H that did not diffuse out of the implanted region during the primary anneal. Figure 5 shows the ^{2}H profiles of the etched B2 sample, before and after annealing at 620 °C for 30 min and 2 h, respectively. ^{2}H has diffused deeper into the samples forming Gaussian shaped profiles, but the integrated ^{2}H dose remains constant showing that no

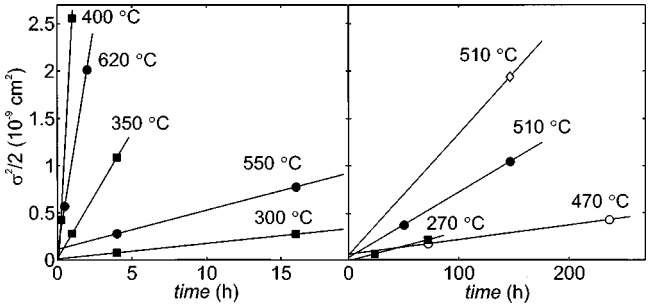

FIG. 7. The Gaussian standard deviations σ, obtained from least square fits to the ^{2}H profiles of the etched and annealed B1 (○), B2 (●), B4 (◇), and Al1 (■) samples, plotted as $\sigma^2/2$ versus the anneal time t. The effective diffusion constant for each sample/temperature combination is given by the slope of the straight line connecting the corresponding $\sigma(t)$. For the B4 sample, with only one extracted σ value, the same $(\sigma^2/2)_{t=0}$ was assumed as for the B1 sample (which has similar B doping).

significant amount of ^{2}H has diffused out through the sample surface. This redistribution of ^{2}H implies a significant dissociation of the ^{2}H-B complexes and the observed diffusion is thus a process of continuous dissociation and formation of ^{2}H-B complexes as discussed in Sec. II A. According to Eq. (9), the total ^{2}H concentration, $[^2\mathrm{H}_{\mathrm{tot}}]$, should, once a local equilibrium has been established between complex formation and dissociation, diffuse according to Fick's law with a constant effective diffusivity D_{eff}. The Gaussian shapes of the profiles in Fig. 5 support this since the solution of Fick's diffusion equation with an initial delta-shaped profile, just inside a reflective boundary at $x=x_0$, is a Gaussian function centered around x_0. The Gaussian standard deviation σ is related to the diffusivity as $D_{\mathrm{eff}}=\sigma^2/2t$.[39] The redistribution of ^{2}H in the etched and annealed Al1 samples (Fig. 6) show the same characteristic Gaussian profiles as for the B samples, with the difference that the ^{2}H atoms pile up at the deeper interface of the buried Al layer (350 °C for 4 h profile in Fig. 6). The pileup and conservation of the ^{2}H dose demonstrate that both interfaces of the Al layer act as reflective boundaries. Numerical simulations show that this can be explained solely by trap limited diffusion but the pile-up will be further pronounced by the built-in electric field at the Al layer edges, directed so that the mobile $^2\mathrm{H}^+$ are ''trapped'' in the layer.[26] Figure 6 also reveals an unexpected accumulation of ^{2}H in the surface region ($x\leqslant0.25\,\mu$m) of the etched and annealed Al1 samples; one explanation may be that ^{2}H has formed stable complexes with defects induced by the plasma etch. Indeed, such defects in SiC have been recently reported by several groups.[15,18] To extract D_{eff}, Gaussian functions are fitted to the ^{2}H profiles. For the Al1 samples the sum of two Gaussian functions are used, with equal σ and with the second Gaussian centered around $x=2.4\,\mu$m, to account for the deeper reflective boundary at $x=1.4\,\mu$m. The fitted Gaussian functions are displayed in Figs. 5 and 6 as solid lines and exhibit good agreement to the SIMS profiles. Equally good fits were obtained for all profiles used in the extractions of D_{eff}. However, it should be mentioned that ^{2}H profiles in B1 samples, annealed to obtain considerably

TABLE III. Effective ^{2}H diffusion constants D_{eff} extracted from the B1, B2, B4, and Al1 samples at anneal temperature T. the ^{2}H-B (B1, B2, B4) and ^{2}H-Al (Al1) dissociation frequencies ν are calculted from D_{eff} using Eq. (10b) with respective trap concentration given in Table I.

Sample	T (°C)	D_{eff} (cm^2/s)	ν (s^{-1})
B1	470	4.3×10^{-16}	1.2×10^{-4}
B2	510	1.9×10^{-15}	7.4×10^{-4}
B4	510	3.6×10^{-15}	7.8×10^{-4}
B2	550	1.1×10^{-14}	4.2×10^{-3}
B2	620	2.7×10^{-13}	9.1×10^{-2}
Al1	270	8.7×10^{-16}	8.1×10^{-3}
Al1	300	4.6×10^{-15}	4.1×10^{-2}
Al1	350	7.5×10^{-14}	6.1×10^{-1}
Al1	400	7.9×10^{-13}	5.9×10^{0}

shorter diffusion lengths than those in Fig. 5, could not be explained by Fickian diffusion and a constant diffusivity. This is most likely due to the addition of a drift component to the ^{2}H diffusion, imposed by the band bending towards the surface and/or the gradient of active doping as a result of the ^{2}H passivation. With deeper penetration of the ^{2}H and the subsequent decrease of the passivation, these effects can be neglected as confirmed by the Gaussian shapes of the (deeper) profiles. Further indications of a surface induced electric field can be found in Fig. 5, where a depletion of ^{2}H in the near surface region ($x \leqslant 90$ nm) of the annealed samples occurs. As an example, if a surface band bending of -1 eV is assumed, roughly pinning the Fermi level to the middle of the band gap at the surface, this field would extend 60 nm into the annealed B2 samples and add an inward drift component to the mobile $^2H^+$. The -1 eV band bending would therefore also account for the reflective boundary at the sample surface of the B samples.

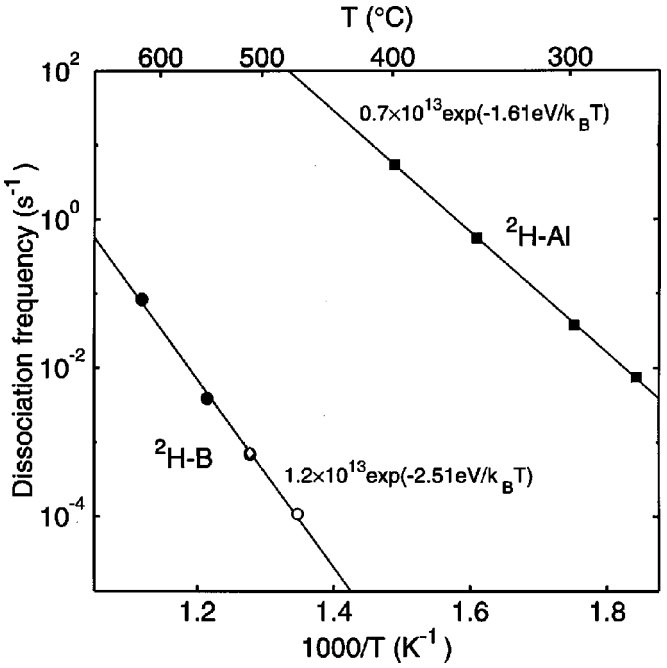

FIG. 8. Arrhenius plot of the dissociation frequencies obtained from the B1 (○), B2 (●), B4 (◇), and Al1 (■) samples. The least square fits of Arrhenius equations (solid lines) to the 4H-SiC samples (B1, B2, and Al1) yield the ^{2}H-acceptor complex dissociation energies: $E_d^{\text{HB}}=(2.51\pm0.04)$ eV and $E_d^{\text{HAl}}=(1.61\pm0.02)$ eV. The extracted dissociation attempt frequencies: $\nu_0^{\text{HB}}=(1.2\pm0.7)\times10^{13}\,\text{s}^{-1}$ and $\nu_0^{\text{HAl}}=(0.7\pm0.3)\times10^{13}\,\text{s}^{-1}$, are very close to the characteristic oscillation frequency of the SiC lattice, $\nu_{\text{lattice}}^{\text{SiC}}=1.6\times10^{13}\,\text{s}^{-1}$. The error limits are the sum of the random errors, obtained from the fittings, and the systematic experimental errors. The ^{2}H-B dissociation frequency from the 6H-SiC sample (B4) agrees with that of the 4H-SiC sample (B2).

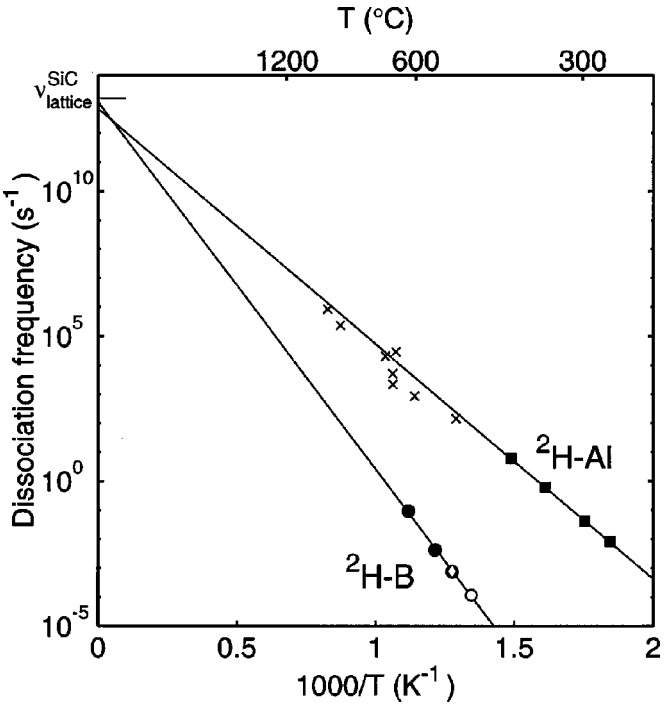

FIG. 9. Arrhenius plot of the H-acceptor dissociation frequencies extrapolated to 1000/T=0. The experimental dissociation frequencies (○, ●, ◇, and ■) and the Arrhenius equations (solid lines) are the same as in Fig. 8. The characteristic oscillation frequency of the SiC lattice, $\nu_{\text{lattice}}^{\text{SiC}}=1.6\times10^{13}\,\text{s}^{-1}$, is indicated at the ordinate and display the close agreement of the extracted dissociation attempt frequencies and $\nu_{\text{lattice}}^{\text{SiC}}$. The dissociation frequencies deduced from the diffusion constants of ^{3}H in highly Al doped SiC in Ref. 27 (×), closely follow the predicted Arrhenius dependence of the ^{2}H-Al dissociation frequencies.

The extracted values of σ are plotted as $\sigma^2/2$ versus t in Fig. 7 and D_{eff} is determined as the slope of the straight line connecting the two data points at each temperature and sample combination. The extrapolated lines of all Al1 samples, and of all B1 and B2 samples, intercept the ordinate at a common point: $(\sigma^2/2)_{t=0}\approx0.0$, and $0.1\times10^{-9}\,\text{cm}^2$, respectively. This confirms the $\sqrt{t}$ evolution of the diffusion process. For sample B4 only one annealing was performed and D_{eff} was here extracted by forcing the line through the ordinate at a the same point as for the B1 and B2 samples. This is not expected to add any significant error to this D_{eff}

value considering the large value of σ for sample B4. The extracted D_{eff} values are listed in Table III and demonstrate a large difference when comparing the B- and Al-doped samples; similar values are obtained, but at an approximate temperature difference of 200 °C.

In the following discussion, we will assume that all extracted D_{eff} are limited by the trapping and dissociation processes as expressed by Eq. (10b), i.e., that the concentration of trapped ^{2}H dominate over the amount of mobile ^{2}H. This seems to make sense at least for the B samples considering the negligible dissociation of the ^{2}H-B complexes at a temperature not too far below the annealing temperature of the etched samples. Furthermore, the big difference in the temperature dependence of the extracted D_{eff} between the B and Al doped samples makes it unlikely that D_{eff} would be identical to the intrinsic hydrogen diffusivity D_{H} [Eq. (10a)]. We will present a more formal proof for this assumption later in this section. Using Eq. (10b) the ^{2}H-B and ^{2}H-Al dissociation frequencies are deduced from the effective diffusion constants. The trap concentration B_{tot} is set to the chemical B and Al concentrations given in Table I; hereby, we assume that the concentration of ^{2}H-Al complexes in the B samples is negligible compared to that of ^{2}H-B. R is set to the Coulomb force assisted R_c of Eq. (3), in accordance with the experimental findings described in Sec. IV A. The extracted frequencies are listed in Table III and are displayed in Fig. 8 together with least square fits of Eq. (4) for the 4H-SiC samples. The fitted Arrhenius equations display excellent agreement over the three orders of magnitude covered by the experimental ν^{HB} and ν^{HAl}, respectively. The fits yield the dissociation energies $E_d^{\text{HB}}=(2.51\pm0.04)$ eV and $E_d^{\text{HAl}}=(1.61\pm0.02)$ eV, and the attempt frequencies $\nu_0^{\text{HB}}=(1.2\pm0.7)\times10^{13}\,\text{s}^{-1}$ and $\nu_0^{\text{HAl}}=(0.7\pm0.3)\times10^{13}\,\text{s}^{-1}$, for the ^{2}H-B and ^{2}H-Al complexes, respectively. The error limits represent the sum of the random errors, obtained from the 99% confidence interval in the Arrhenius fitting procedure, and of the systematic errors, from the uncertainty in annealing temperature ($\Delta T\leqslant5$ °C), in absolute concentrations of the SIMS measurements (20%), and from the error in the effective capture radius ($\Delta R/R=20\%$).

The extracted attempt frequencies are very close to the theoretical characteristic oscillation frequency of the SiC lattice obtained in Sec. II A, $\nu_{\text{lattice}}^{\text{SiC}}=1.6\times10^{13}\,\text{s}^{-1}$. The agreement of the two ν_0 values and $\nu_{\text{lattice}}^{\text{SiC}}$ is quite remarkable considering the extrapolations over 13 orders of magnitude in the determination of ν_0 and the large difference between E_d^{HB} and E_d^{HAl}, as clearly illustrated in Fig. 9. It should be mentioned that the agreement between the experimental ν_0 values for the H-acceptor dissociation frequencies and the theoretical ν_{lattice} is not unique for SiC. Dissociation attempt frequencies in high 10^{12} to the low $10^{14}\,\text{s}^{-1}$ range have been reported for H-acceptor and H-donor complexes in both Si (Ref. 3) and GaAs.[40] However, the dissociation energy for the ^{2}H-B complex is almost 1 eV larger than for ^{2}H-Al which shows that the atomic configurations of the two complexes must be quite different. This large difference in E_d has not been observed in other semiconductors; in Si and GaAs all reported dissociation energies are in the range of 1.15–1.45 eV for both H-acceptor[3,40] and H-donor[40,41] complexes.

Only one dissociation frequency was extracted from the B-doped 6H-SiC sample (B4). However, the spot-on agreement between this value of ν_{HB} and the value obtained from the B2 sample at the same temperature (Table III, Fig. 8) provides strong evidence that the formation and dissociation properties of the ^{2}H-B complex do not differ between 4H-and 6H-SiC.

In the extraction of the dissociation frequencies, D_{eff} was assigned to the trapping/detrapping process, Eq. (10b), and not to the intrinsic hydrogen diffusivity D_{H}, Eq. (10a). The effective diffusivities in the B2 and Al1 samples obey the Arrhenius equations, $D_{\text{eff}}^{\text{B2}}=30\times\exp(-2.5\,\text{eV}/k_B T)$ cm^2/s and $D_{\text{eff}}^{\text{Al1}}=2\times\exp(-1.6\,\text{eV}/k_B T)$ cm^2/s, respectively, which gives $D_{\text{eff}}^{\text{Al1}}>10^5\times D_{\text{eff}}^{\text{B2}}$ at 450 °C. Considering that the total acceptor doping concentration is less than a factor of 10 higher in Al1 than in B2, a Fermi level dependence is not plausible to account for this large difference in D_{eff}. Furthermore, the close resemblance of ν_0^{HB} and ν_0^{HAl}, to $\nu_{\text{lattice}}^{\text{SiC}}$ does indeed support the assignment of D_{eff} to the trapping/detrapping process. For the B samples it was assumed that the [^{2}H$_{\text{tot}}$] profiles were predominantly composed of ^{2}H-B complexes although Al was present in these samples at a concentration comparable to B. This assumption hold with a high degree of validity since the LE concentration ratio of two complexes with common mobile species [^{2}H], equal trap concentrations ([B] and [A]), and equal R, is given by the inverse ratio of the complex dissociation frequencies, i.e., $[^2\text{H-B}]/[^2\text{H-Al}]=\nu^{\text{HAl}}/\nu^{\text{HB}}\approx\exp(0.9\,\text{eV}/k_B T)=3\times10^5$ at 550 °C.

In the extraction of the effective capture radius R^{HB} in Sec. IV A it was assumed that (i) the dissociation frequency was sufficiently low for Eq. (14) to be valid, and (ii) that the nonconstant concentration of mobile ^{2}H at the ''surface,'' ^{2}H$_0$, did not affect the exponential profiles of the diffusion fronts. To verify these assumptions computer simulations for the implanted and 460 °C primary annealed B1 samples were performed by solving Eq. (2) numerically, with boundary condition (12) ($x_{\text{surface}}=0.24\,\mu$m) and $R=R_c$, $\nu=\nu^{\text{HB}}$, and $B_{\text{tot}}=$[B]. Neither D_{H} nor ^{2}H$_0$ are known, but since the depth of ^{2}H penetration L, Eq. (18), as well as the condition for negligible dissociation, Eq. (11), both depend on the product ($D_{\text{H}}\times{}^2\text{H}_0$), it is possible to postulate one of them and treat the other as a fitting parameter. With ^{2}H$_0$ set to $^2\text{H}_0^1=10^{15}\,\text{cm}^{-3}$ during the first simulated 30 min, $D_{\text{H}}=1.8\times10^{-11}\,\text{cm}^2/\text{s}$ provided the closest fit to the experimental data. ^{2}H$_0$ was then abruptly lowered to $^2\text{H}_0^2=1\times10^{14}\,\text{cm}^{-3}$ during the following 90 min to account for the nonideal diffusion source; D_{H} was kept unchanged. Several combinations of $^2\text{H}_0^{1,2}$ and D_{H} were tried giving identical [^{2}H$_{\text{tot}}$] profiles as long as the product ($D_{\text{H}}\times{}^2\text{H}_0^1$) and the ratio ($^2\text{H}_0^1/{}^2\text{H}_0^2$) were preserved (within the limit of $^2\text{H}_0^1\ll[^2\text{H}_{\text{tot}}]$). The simulated profiles are displayed in Fig. 3 and the close fits to the SIMS profiles show that the analytical treatment of the diffusion fronts employed in Sec. VI A is justified.

Finally, the extensive amount of data from the present study of the H-acceptor complex formation and dissociation

kinetics support previous brief reports suggesting a maximum dissociation energy of 1.8 eV for the H-Al complex[24] and a higher thermal stability for the H-B complex.[22] Moreover, in a study by Causey *et al.*[27] the activation energy for ^{3}H diffusion in highly Al doped $(6\times10^{20}\,\mathrm{cm}^{-3})$ α-SiC was determined to $(1.48\pm0.18\,\mathrm{eV})$. Since this value resembles the ^{2}H-Al dissociation energy, it seems plausible that the diffusion observed in Ref. 27 was governed by the same trap limited mechanism as in our study. Using the ^{3}H diffusivities from Ref. 27, the corresponding ^{3}H-Al dissociation frequencies are deduced from Eq. (10b) with $B_{\mathrm{tot}}=6\times10^{20}\,\mathrm{cm}^3$ and $R=R_c$. As can be seen in Fig. 8 these frequencies closely follow the predicted Arrhenius dependence of ν^{HAl}. Hence, once again the universality of the trap limited diffusion mechanism for H in acceptor doped SiC is demonstrated and the agreement is quite remarkable, not only considering the more than three orders of magnitude difference in Al concentration but also the very different experimental procedures of the two investigations.

V. SUMMARY

In this work we have presented a detailed experimental study of ^{2}H diffusion, it's complex formation, and subsequent dissociation, with B and Al in *p*-type 4*H*- and 6*H*-SiC. Furthermore, in Sec. I we reviewed the main published data on this subject and in Sec. II we gave a detailed theoretical survey of the trap limited diffusion kinetics related to the diffusion of H in acceptor doped semiconductors. Our main results can be summarized as follows.

(1) ^{2}H diffusion in *p*-type SiC follows the kinetics expected for a trap limited diffusion mechanism with formation and dissociation of ^{2}H-B and ^{2}H-Al complexes, respectively. (2) The effective capture radius between ^{2}H and B at 460 °C, extracted from ^{2}H depth profiles characterized by negligible dissociation of the ^{2}H-B complexes, has been determined to $R^{\mathrm{HB}}=(21\pm4)$ Å. This relatively large value indicates that the trapping occurs via Coulomb attraction between H^+ and B^- and agrees with the value obtained from the expression $e^2/(4\pi R_c)=k_BT\Rightarrow R_c=23$ Å. (3) By measuring the effective H diffusivity in B- and Al-doped 4*H*-SiC epitaxial layers, the respective ^{2}H-B and ^{2}H-Al complex dissociation frequencies were determined. The extracted frequencies covered three orders of magnitude and displayed excellent Arrhenius dependence. The complex dissociation energies from the Arrhenius fits yielded $E_d^{\mathrm{HB}}=(2.51\pm0.04)$ eV and $E_d^{\mathrm{HAl}}=(1.61\pm0.02)$ eV. The large difference in E_d shows that the atomic configurations of the two complexes are significantly different in contrast to that observed for other semiconductors. (4) The close resemblance between the extracted dissociation attempt frequencies, $\nu_0^{\mathrm{HB}}=(1.2\pm0.7)\times10^{13}\,\mathrm{s}^{-1}$ and $\nu_0^{\mathrm{HAl}}=(0.7\pm0.3)\times10^{13}\,\mathrm{s}^{-1}$, and the characteristic oscillation frequency of the SiC lattice, $\nu_{\mathrm{lattice}}^{\mathrm{SiC}}=1.6\times10^{13}\,\mathrm{s}^{-1}$, validates the assumption of a first order dissociation process. (5) One dissociation frequency for B-doped 6*H*-SiC was determined and found to be identical with that for the B-doped 4*H*-SiC samples. This suggests strongly that the properties of the H-acceptor trap limited diffusion mechanism do not differ between the two polytypes.

ACKNOWLEDGMENTS

The authors are grateful to Stefan Karlsson and Nils Nordell for providing the SiC epitaxial layers, and to Erik Danielsson for assistance with the ICP plasma etch. This work was funded by the Swedish Foundation for Strategic Research, within the SiCEP program.

[1] J. I. Pankov and N. M. Johnson, *Hydrogen in Semiconductors* (Academic, New York, 1991).
[2] S. J. Pearton, J. W. Corbett, and M. Stavola, *Hydrogen in Crystalline Semiconductors* (Springer-Verlag, New York, 1991).
[3] T. Zundel and J. Weber, Phys. Rev. B **39**, 13549 (1989).
[4] T. Zundel and J. Weber, Phys. Rev. B **46**, 2071 (1992).
[5] A. G. Acheson, Engl. Pat. 17911 (1892) and W. F. Knippenberg, Philips Res. Rep. **18**, 161 (1963).
[6] R. Siegele, S. P. Withrow, J. Roth, and B. M. U. Scherzer, J. Nucl. Mater. **176&177**, 1010 (1990).
[7] See, for example, W. J. Choyke and G. Pensl, MRS Bull. **22**, 25 (1997).
[8] N. Nordell, A. Schöner, and S. G. Andersson, J. Electrochem. Soc. **143**, 2910 (1996).
[9] D. J. Larkin, S. G. Sridhara, and W. J. Choyke, J. Electron. Mater. **24**, 289 (1995).
[10] A. Schöner, K. Rottner, N. Nordell, M. K. Linnarsson, C. Peppermüller, and R. Helbig, Diamond Relat. Mater. **6**, 1293 (1997).
[11] J. Portman, C. Haug, R. Brenn, J. Schneider, K. Rottner, and R. Helbig, Nucl. Instrum. Methods Phys. Res. B **155**, 132 (1999).
[12] F. Gendron, L. M. Porter, C. Porte, and E. Bringuier, Appl. Phys. Lett. **67**, 1253 (1995).
[13] B. Clerjaud, F. Gendron, C. Porte, and W. Wilkening, Solid State Commun. **95**, 463 (1995).
[14] B. Theys, F. Gendron, C. Porte, E. Bringuier, and C. Dolin, J. Appl. Phys. **82**, 6346 (1997).
[15] A. O. Konstantinov, P. A. Ivanov, O. I. Kon'kov, and E. I. Terukov, in *Fifth International Conference on Silicon Carbide and Related Materials*, edited by M. G. Spencer, R. P. Devaty, J. A. Edmond, M. A. Khan, R. Kaplan, and M. Rahman, IOP Conf. Ser. Proc. No. 137 (IOP, Bristol, 1994), p. 275.
[16] G. J. Gerardi, E. H. Pointdexter, and D. J. Keeble, Appl. Spectrosc. **50**, 1428 (1996).
[17] F. Ren, J. M. Grow, M. Bhaskaran, R. G. Wilson, and S. J. Pearton, J. Electron. Mater. **26**, 198 (1996).
[18] G. McDaniel, J. W. Lee, E. S. Lambers, S. J. Pearton, P. H. Holloway, F. Ren, J. M. Grow, M. Bhaskaran, and R. G. Wilson, J. Vac. Sci. Technol. A **15**, 885 (1997).
[19] M. K. Linnarsson, M. Janson, A. Schöner, N. Nordell, S. Karlsson, and B. G. Svensson, in *International Conference on SiC, III-Nitrides and Related Materials, 1997*, edited by G. Pensl, H. Morkoc, B. Monemar, and E. Janzén, Mater. Sci. Forum Proc. No. 264–268 (Trans Tech Publ., Switzerland, 1998), p. 761.

[20] M. K. Linnarsson, M. Janson, S. Karlsson, A. Schöner, N. Nordell, and B. G. Svensson, Mater. Sci. Eng., B **61-62**, 275 (1999).
[21] M. K. Linnarsson, A. L. Spetz, M. S. Janson, L. G. Ekdahl, S. Karlsson, A. Schöner, I. Lundström, and B. G. Svensson, in *International Conference on SiC and Related Materials 1999*, edited by J. C. H. Carter, R. P. Devaty, and G. S. Roher, Mater. Sci. Forum Proc. No. 338-342 (Trans Tech Publ., Switzerland, 2000), p. 937.
[22] N. Achtziger, J. Grillenberger, W. Witthuhn, M. K. Linnarsson, M. Janson, and B. G. Svensson, Appl. Phys. Lett. **73**, 945 (1998).
[23] N. Achtziger, C. Hülsen, W. Witthuhn, M. K. Linnarsson, M. Janson, and B. G. Svensson, Phys. Status Solidi B **210**, 395 (1998).
[24] C. Hülsen, N. Achtziger, U. Reislöhner, and W. Witthun, in *International Conference on Silicon Carbide and Related Materials*, edited by J. C. H. Carter, R. P. Devaty, and G. S. Roher, Mater. Sci. Forum Proc. No. 338-342 (Trans Tech Publications, Switzerland, 2000), p. 929.
[25] M. S. Janson, A. Hallén, M. K. Linnarsson, N. Nordell, S. Karlsson, and B. G. Svensson, in *European Conference on SiC and Related Materials 2000*, edited by G. Pensl, D. Stephani, and M. Hundhausen, Mater. Sci. Forum Proc. No. 353–356 (Trans Tech. Publ., Switzerland, 2001), p. 353.
[26] M. S. Janson, M. K. Linnarsson, A. Hallén, B. G. Svensson, N. Nordell, and S. Karlsson, Phys. Rev. B **61**, 7195 (2000).
[27] R. A. Causey, J. D. Fowler, C. Ravanbakht, T. S. Elleman, and H. Verghese, J. Am. Ceram. Soc. **61**, 221 (1978).
[28] M. A. Roberson and S. K. Estreicher, Phys. Rev. B **44**, 10578 (1991).
[29] P. Deák, A. Gali, and B. Aradi, in *European Conference on SiC and Related Materials 2000*, edited by G. Pensl, D. Stephani, and M. Hundhausen, Mater. Sci. Forum Proc. No. 353–356 (Trans Tech Publ., Switzerland, 2001), p. 421.
[30] A. Gali, B. Aradi, and P. Deák, Phys. Rev. Lett. **84**, 4926 (2000).
[31] A. Fick, Ann. Phys. (Leipzig) **170**, 59 (1855).
[32] T. R. Wait, J. Chem. Phys. **28**, 103 (1958).
[33] J. J. Thomson, Philos. Mag. **47**, 337 (1924).
[34] A. Zywietz, K. Karch, and F. Bechstedt, Phys. Rev. B **54**, 1791 (1995).
[35] C. H. Seager, R. A. Anderson, and D. K. Brice, J. Appl. Phys. **68**, 3268 (1990).
[36] A. Henry, B. Magnusson, M. K. Linnarsson, A. Ellison, M. Syväjärvi, R. Yakimova, and E. Janzén, in *European Conference on SiC and Related Materials 2000*, edited by G. Pensl, D. Stephani, and M. Hundhausen, Mater. Sci. Forum Proc. No. 353–356 (Trans. Tech. Publ., Switzerland, 2001), p. 373.
[37] M. K. Linnarsson, J. P. Doyle, and B. G. Svensson, in *III-Nitride, SiC and Diamond Materials for Electronic Devices*, edited by D. K. Gaskill, C. D. Brandt, and R. J. Nemanich, Mater. Res. Soc. Symp. Proc. No. **423** (Materials Research Society, Pittsburgh, 1996), p. 635.
[38] M. Janson, M. K. Linnarsson, A. Hallén, and B. G. Svensson, in *Hydrogen in Semiconductors and Metals*, edited by N. H. Nickel, W. B. Jackson, R. C. Bowman, and R. G. Leisure, Mater. Res. Soc. Symp. Proc. No. **513** (Materials Research Society, Warrendale, 1998), p. 439.
[39] J. Philibert, *Atom Movements Diffusion and Mass Transport in Solids* (Les Éditions de Physique, Les Ulis, France, 1991).
[40] S. J. Pearton, C. R. Abernathy, and J. Lopata, Appl. Phys. Lett. **59**, 3571 (1991).
[41] J. Zhu, N. M. Johnson, and C. Herring, Phys. Rev. B **41**, 12354 (1990).